

Article

# Quantifying DOC and Its Controlling Factors in Major Arctic Rivers during Ice-Free Conditions using Sentinel-2 Data

Jue Huang<sup>1,\*</sup>, Ming Wu<sup>1</sup>, Tingwei Cui<sup>2</sup> and Fanlin Yang<sup>1</sup>

<sup>1</sup> College of Geomatics, Shandong University of Science and Technology, Qingdao 266590, China; wuming1016@sdust.edu.cn (M.W.); flyang@sdust.edu.cn (F.Y.)

<sup>2</sup> First Institute of Oceanography, Ministry of Natural Resources, Qingdao 266061, China; cuitingwei@fio.org.cn

\* Correspondence: huangjue@sdust.edu.cn

Received: 30 September 2019; Accepted: 3 December 2019; Published: 5 December 2019



**Abstract:** The six largest Arctic rivers (Yenisey, Lena, Ob', Kolyma, Yukon, and Mackenzie) drain the organic-rich Arctic watersheds and serve as important pools in the global carbon cycle. Satellite remote sensing data are considered to be a necessary supplement to the ground-based monitoring of riverine organic matter circulation, especially for the ice-free periods in high-latitudes. In this study, we propose a remote sensing retrieval algorithm to obtain the chromophoric dissolved organic matter (CDOM) levels of the six largest Arctic rivers using Sentinel-2 images from 2016 to 2018. These CDOM results are converted to dissolved organic carbon (DOC) concentrations using the strong relationship ( $R^2 = 0.89$ ) between the field measurements of these two water constituents. The temporal-spatial distributions of the DOC in the six largest Arctic rivers during ice-free conditions are depicted. The performance of the retrieval algorithm verifies the capacity of using Sentinel-2 data to monitor riverine DOC variations due to its improved spatial resolution, better band placement, and increased observation frequency. River discharge, watershed slopes, human activities, and land use/land cover change drove much of the variation in the satellite-derived DOC. The seasonality, geography, and scale would affect the correlation between DOC concentration and these influence factors. Our results could improve the ability to monitor DOC fluxes in Arctic rivers and advance our understanding of the Earth's carbon cycle.

**Keywords:** chromophoric dissolved organic matter; dissolved organic carbon; Arctic rivers; Sentinel-2

## 1. Introduction

The Arctic Ocean (AO), containing only ~1% of the global ocean volume, could receive ~10% of the annual global riverine discharge. A large part (~60%) of the discharge stems from the six largest Pan-Arctic rivers, which transport significant quantities of organic matter into the AO [1,2]. Through their direct impacts on water overland runoff, terrestrial processes may influence the biogeochemical attributes of the Arctic Regions. Recent studies have revealed the significant changes in the Arctic terrestrial ecosystem as a key characteristic of global climate change. Researchers have paid great attention to the largest temperature changes at high latitudes [3], the rapid reduction in sea ice and spring snow-cover [4], widespread permafrost degradation [5], and various alterations in biogeochemical circles in Arctic Regions [6].

As an important pool in the Arctic carbon cycle, riverine dissolved organic carbon (DOC) tightly links terrestrial and marine systems and also markedly modifies the biogeochemical characteristics of the AO waters. With the progress of global warming, the permafrost in the Arctic is undergoing remarkable thawing, which is likely to alter more than half of the soil organic carbon stock on Earth

that is stored in the permafrost [7]. However, recent studies on DOC concentrations have revealed contrasting responses to climate change in different Arctic rivers [1,8]. The reasons for these responses can be attributed to the biological utilization of and photochemical interactions with DOC, but their relative importance and influencing factors remain very uncertain [1].

The coordinated sampling efforts of the important Arctic rivers have provided the necessary materials for studies of riverine DOC. With the help of the USGS Load Estimator (LOADEST), a discharge-constituent flux regression model and the multiyear field datasets from PARTNERS/Arctic-GRO [9,10] have been used to establish several discharge-DOC relationships [11–13]. Based on these field-measured data, many previous studies have examined the source and variation of DOC, and river discharge, topography, and land cover were considered to be major influencing factors [14–18]. Other researchers determined the source and flux variation of DOC by analyzing spectral or absorption characteristics of chromophoric dissolved organic matter (CDOM) [16,19–22]. However, the field measurements are inevitably constrained by the limited accessibility of sampling sites, especially throughout the ice breakup period [3]. In addition, passive optical remote sensing could provide a relevant data source for the spatial-temporal variations in the DOC concentration that is independent of discharge to supplement field measurements. Using a simple optical measurement, the DOC distribution can be traced with the help of CDOM, which is the light-sensitive portion of the dissolved organic matter (DOM) pool [11,23]. The CDOM/DOC retrieval method has been successfully applied in DOC monitoring of rivers [24,25], lakes [19,26–28], and coastal waters [29,30].

Many efforts have been made to map CDOM/DOC using remotely sensed imagery in different optically complex waters [31–33] with various sensors. Multiband linear or nonlinear combination algorithms have been widely used as CDOM remote sensing retrieval algorithms in different complex waters [3,24,28,31,34,35]. Then, DOC concentration could be obtained from the retrieved CDOM with the help of a CDOM retrieval algorithm [25,34]. However, due to the strong dependency of field-measured data, these algorithms usually need modification before being applied to a new study area or new remote sensing data.

Ocean color remote sensing satellite sensors, such as SeaWiFS, MODIS, or MERIS, benefit from high time resolutions, but their spatial resolutions are too low to evaluate CDOM/DOC variations in rivers. By contrast, high spatial resolution sensors, such as the Landsat Thematic Mapper (TM) and Operational Land Imager (OLI), have appropriate spatial resolutions but are too coarse in terms of repeat orbit cycles. Launched in 2015, the Sentinel-2 mission has provided both high spatial and temporal resolution images for water quality monitoring in waters with dynamic variations and small areas. The successful application of Sentinel-2 images to estimate suspended sediment, chlorophyll, turbidity, and CDOM in lakes, rivers, and coastal waters [36,37] indicated that appropriate remote sensing methods could be developed for CDOM/DOC monitoring in Arctic rivers.

Existing studies have demonstrated that temperature, precipitation, wetland and permafrost coverage, watershed slopes, river discharge, and seasonal thaw play major roles in regulating the variation of DOC in high-latitude catchments [17,38,39]. Previous studies have shown that river discharge played a crucial role in regulating riverine DOC concentration [11,24,40–43]. Other studies indicated that watershed slopes and permafrost depth also played a role in adjusting DOC concentration [39,44–47]. However, few studies have focused on the quantitative analysis of these factors covering the watersheds of the six largest rivers and their sub-watersheds in Arctic regions. In addition, Land-Use and Land-Cover Change (LUCC) also has been highlighted as a promising indicator of DOC variations [47,48]. However, due to the limited coverage of field-measured data and the low spatial resolution of the MODIS-based LUCC that was used in previous studies, the quantitative relationship between the DOC and the LUCC in the Pan-Arctic region has not been reported.

This paper aimed to discuss the potential of Sentinel-2 images with high spatial-temporal resolution for monitoring DOC concentration in Pan-Arctic regions. Here, we proposed the first remote sensing retrieval model that obtained the CDOM concentrations in the six largest Arctic rivers using Sentinel-2 images. These CDOM results were then converted to DOC concentrations using a strong relationship

between these two water constituents. The spatial-temporal variation of DOC between 2016 and 2018 in the six largest Arctic rivers and 35 sub-catchments were revealed. We quantitatively analyzed the influence of river discharge, watershed slopes, human activities, and LUCC on DOC variation at a high spatial resolution. This paper verified the applicability of Sentinel-2 remote sensing data for monitoring DOC fluxes in Arctic rivers. The results presented here not only expanded the scope of DOC research to important sub-catchments in the Arctic but also provided a better understanding of the circulation of riverine DOC in Pan-Arctic regions.

## 2. Methods and Datasets

### 2.1. Field Measured Data

The field measured data of the six largest Arctic rivers from 2003 to 2018 were obtained from the Arctic-GRO and PARTNERS projects ([www.Arcticgreativers.org](http://www.Arcticgreativers.org)). The geographic features and population density of each watershed were described on the website. Water samples were measured at Dudinka (66.48°N, 86.15°E, Yenisey), Zhigansk (66.77°N, 123.37°E, Lena), Salekhard (66.63°N, 66.60°E, Ob'), Cherskiy (68.75°N, 161.30°E, Kolyma), Pilot Station (61.93°N, 162.88°W, Yukon), and Tsiigehtchic (67.45°N, 133.74°W, Mackenzie) near the estuaries of each river (Figure 1). These six Arctic rivers represent 67% of the AO watershed [49]. According to previous studies [43,49], the vertical distributions of all the dissolved chemical constituents are uniform throughout the water column, which is based on a comparison between surface samples and delamination samples.

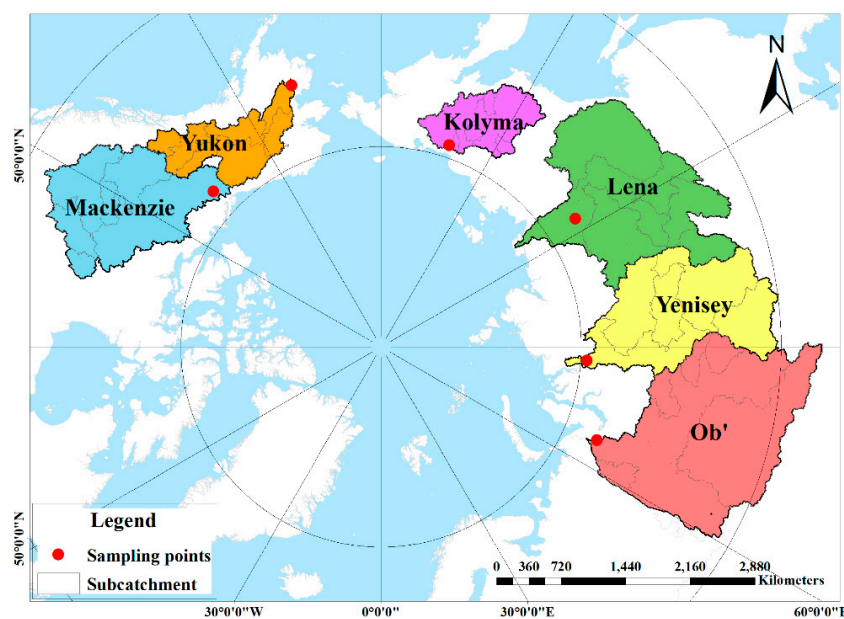


**Figure 1.** Map of the study area with delineated watershed boundaries of the six largest Arctic rivers (black lines), watershed boundaries of sub-catchments (gray lines), and sample locations (red dots).

The DOC and CDOM water samples were filtered through a Geotech capsule filter or an Aquaprep 600 capsule filter into pre-cleaned HDPE bottles and frozen before analysis [11]. The DOC samples from PARTNERS (2003–2006) were analyzed using Atomic Mass Spectrometry (AMS), while the DOC samples from all three Arctic-GRO campaigns were measured using a Shimadzu TOC/TN analyzer. The absorbance ( $A(\lambda)$ ) was measured using a Shimadzu UV-1800 spectrophotometer in a 1 cm quartz cell from 200 to 800 nm at a 1 nm interval. Although the frozen water samples might lead to changes in

the CDOM, previous studies found minimal effects of freezing on the dissolved organic matter [11]. The  $A(\lambda)$  was converted to absorption coefficient as follows:

$$a(\lambda) = 2.303A(\lambda)/l, \quad (1)$$

where  $a(\lambda)$  is the absorption coefficient ( $\text{m}^{-1}$ ), and  $l$  is the cell path length (m). The  $a(\lambda)$  at 254, 375, or 440 nm are often used as proxies for the CDOM. Specific ultraviolet absorbance ( $\text{SUVA}_{254}$ ,  $\text{L mg C}^{-1} \text{m}^{-1}$ ) is defined as the UV absorbance at 254 nm ( $\text{m}^{-1}$ ) divided by the DOC concentration ( $\text{mg L}^{-1}$ ) [50].

Unfiltered water samples were stored chilled in HDPE bottles before measurement. These water samples were filtered through pre-weighed GF/F filters and were weighed after drying for 24 h at 60 °C. The total suspended sediment (TSS) concentrations were calculated using the paired weight of each filter and the water volume passing through each filter.

The river discharge data were collected from hydrometric stations at downstream locations on each river, which were obtained from the ArcticRIMS website (<http://rims.unh.edu/data.shtml>) [51]. Detailed descriptions of the collection and measurements can be found in previous studies that used the Arctic-GRO/PARTNERS project [43,48,49]. The statistics of the field-measured data used in this study are listed in Table 1.

**Table 1.** Statistics of field measured data.

River		Discharge $\text{m}^3/\text{s}$	Temperature $^{\circ}\text{C}$	CDOM $\text{m}^{-1}$	DOC $\text{mg C/L}$	TSS $\text{mg/L}$	$\text{SUVA}_{254}$ $\text{L mg C}^{-1} \text{m}^{-1}$
Yenisey	Min	5850	−1.00	0.010	2.20	0.15	1.861
	Max	98,500	18.00	0.086	12.96	26.10	4.163
	Mean	26,417	7.00	0.037	6.34	5.78	3.109
Lena	Min	2076	−0.50	0.017	3.20	0.59	2.187
	Max	163,000	19.90	0.129	23.50	221.00	4.152
	Mean	34,360	7.30	0.055	9.47	29.80	3.214
Ob'	Min	3350	−2.00	0.013	4.00	1.57	2.019
	Max	36,300	20.00	0.111	16.60	134.80	4.216
	Mean	17,668	6.90	0.061	9.70	31.00	3.301
Kolyma	Min	148	0.00	0.004	2.48	0.35	1.420
	Max	24,300	15.90	0.103	18.40	394.59	3.444
	Mean	5796	6.50	0.025	5.69	46.25	2.398
Yukon	Min	1175	−2.00	0.007	2.10	3.64	1.917
	Max	33,414	19.50	0.109	15.90	863.00	3.747
	Mean	9726	8.40	0.032	5.85	212.44	2.743
Mackenzie	Min	2960	−2.00	0.008	2.27	0.80	1.529
	Max	28,800	19.60	0.052	8.10	461.38	4.442
	Mean	10,900	8.10	0.022	4.66	91.33	2.364

## 2.2. Remote Sensing Image Processing

Sentinel-2 was launched by the European Space Agency (ESA) for land observation. With a high radiation resolution of 12 bits and a high spatial resolution of 10 m, the remote sensing images captured by Sentinel-2 can also play a significant role in water environment research, especially for inland lakes and rivers. The coverage cycle is 10 days with one satellite and 5 days with 2 satellites. All these improvements prompt us to validate the availability of Sentinel-2 for remote sensing measurements in complex water environments. Furthermore, few previous studies have focused on high-range monitoring in Arctic regions using Sentinel-2.

This study utilized Sentinel-2 optical data and in situ data that were in close proximity to achieve synchronous measurements. We inspected the Sentinel-2 remote sensing images from September 2015 to March 2018 in the Arctic regions, and only images with 30% cloud cover or less were retained.

In addition, we guaranteed that the sampling sites had clear skies and were clear of ice/snow cover via visual inspection. However, the frequent cloud and ice/snow cover in the Arctic region inevitably reduced the availability of images in our study area. Consequently, we only obtained 15 images during the ice-free period that were quasi-synchronized with field measurements from the ESA with a maximum time interval of 8 days between remote sensing images and the in-situ data (Table 2). With the help of Sen2cor, a plug-in that was released by the ESA for the production of L2A level data, we acquired the Bottom-of-Atmosphere corrected reflectance without atmospheric influence.

**Table 2.** List of the available Sentinel-2 scenes for modeling the chromophoric dissolved organic matter (CDOM) retrieval algorithm in this study.

Rivers	Acquisition Date of Images	Sampling Date of DOC
Yenisey	17 June 2017	14 June 2017
Lena	02 August 2016	31 July 2016
Lena	29 June 2017	03 July 2017
Lena	02 August 2017	05 August 2017
Ob'	18 June 2017	25 June 2017
Kolyma	04 October 2016	04 October 2016
Kolyma	01 June 2017	28 May 2017
Kolyma	08 August 2017	16 August 2017
Kolyma	03 October 2017	09 October 2017
Yukon	01 September 2016	29 August 2016
Yukon	24 August 2017	18 August 2017
Yukon	18 October 2017	18 October 2017
Mackenzie	02 October 2016	05 October 2016
Mackenzie	29 June 2017	29 June 2017
Mackenzie	28 August 2017	03 September 2017

### 2.3. Catchment Characteristic Data

The LUCC data used in this study were downloaded from FROM-GLC (Finer Resolution Observation and Monitoring of Global Land Cover, <http://data.ess.tsinghua.edu.cn>) [52]. Based on the free accessibility of Sentinel-2 images and the powerful computing power of the Google Earth Engine cloud platform, FROM-GLC classified the LUCC into 10 categories, including cropland, forest, grassland, shrubland, wetland, water, tundra, impervious surface, bareland, and snow/ice. After conducting optimization using the grid search method and large numbers of LUCC training and validation samples from different seasons, the FROM-GLC data demonstrated strong robustness and high precision with an overall classification accuracy of up to 72.34% [53].

The watershed of each Arctic rivers was delineated using GMTED2010 DEM data (<https://earthexplorer.usgs.gov/>) [54] with a spatial resolution of 7.5 arc seconds, as shown in Figure 1 with black lines. The calculation of the confluence cumulant, the acquisition of the flow length, the classification of the river network, and the definition of the catchment areas were conducted using the Hydrological Analysis tool of ArcGIS 10.5. We not only delineated the catchments of the six largest Arctic rivers but also delineated 35 sub-catchments (grey lines in Figure 1) in order to analyze the topographic features and water properties in different sized watersheds. The details of the methods that were used to define the watershed boundaries can be found in [39].

The population of each watershed was calculated from ORNL's LandScan™ 2017 datasets released by Oak Ridge National Laboratory (<https://landscan.ornl.gov/landscan-datasets>) [55] in 2017. At approximately 1 km (30" X 30") spatial resolution, LandScan™ 2017 represented an approximation of the spatial population distribution. With the drainage area delineated above, the population density of each watershed could be obtained.

#### 2.4. CDOM Algorithm Development

According to previous studies [31], the absorption of CDOM exponentially decreases as the wavelength increases, which exerts a more significant influence on the short wavebands, such as the blue band. However, the sensitivity of the blue band in complex waters is easily affected by other water constituents, especially in turbid waters with low reflectance, resulting in atmospheric correction difficulties at the short wavebands. Therefore, longer wavebands would be a better choice for CDOM retrieval in turbid inland waters. Due to the complex biological optical properties of inland waters, band combinations rather than single bands could capture the subtle variations in the driving factors of the CDOM. Previous studies successfully used combinations of the blue, green, and red bands of Landsat and SPOT to calculate the CDOM in coastal waters, rivers, and lakes [3,11,28,56]. Compared to the satellite data that were mentioned above, the spectral, spatial, and temporal improvements of Sentinel-2 data are expected to play crucial roles in the remote sensing monitoring of inland waters. Using the CDOM proxies, absorption coefficients at 254, 375, and 440 nm ( $a_{254}$ ,  $a_{375}$ , and  $a_{440}$ ), as dependent variables and the band combinations as the independent variables, we performed a stepwise regression simulation using the visible wavebands of Sentinel-2. Then, we developed a remote sensing retrieval model that obtained the CDOM concentrations in the six largest Arctic rivers using Sentinel-2 data, as shown in Equation (2). In addition, we also evaluated the models that were recently proposed in [3,11,28,57], as shown in Table 3. The B1, B2, B3, and B4 stood for the first four wavebands of Sentinel-2 data.

**Table 3.** Remote sensing retrieval model for CDOM using Sentinel-2 data.

Model	Equation Form	Coefficients				R <sup>2</sup>	MRE %	P Value	RMSE m <sup>-1</sup>
		b <sub>0</sub>	b <sub>1</sub>	b <sub>2</sub>	b <sub>3</sub>				
K2005	$a_{440} = \exp(b_0 + b_1 \times \ln(B3/B4))$	-4.669	-1.868	—	—	0.612	27.48	<0.001	0.388
G2011	$a_{440} = \exp(b_0 + b_1 \times B4 + b_2 \times (B3/B2))$	-4.759	-2.676	0.265	—	0.338	69.96	>0.050	0.506
H2016	$a_{440} = b_0 + b_1 \times B3 + b_2 \times (B3/B4)$	-2.705	-5.185	-1.552	—	0.632	46.07	<0.010	0.005
G2018	$a_{375} = b_0 + b_1 \times B2 + b_2 \times B3 + b_3 \times (B2/B3)$	0.084	-0.373	-0.599	-0.037	0.448	60.34	>0.050	0.007
	$a_{254} = \exp(b_0 + b_1 \times B2 + b_2 \times B2/B4 + b_3 \times \ln(B3/B4))$	-2.012	-7.82	0.838	-1.859	0.791	40.92	<0.001	0.477
This study	$a_{375} = b_0 \times \ln(B2) - b_1$	-0.014	-0.01	—	—	0.556	42.13	>0.010	0.085
	$a_{375} = b_0 + b_1 \times B2 + b_2 \times B3 + b_3 \times \ln(B3/B4)$	0.016	0.098	-0.163	-0.025	0.732	63.21	>0.001	0.123
	<b><math>a_{375} = b_0 + b_1 \times B2 + b_2 \times B2/B4 + b_3 \times \ln(B3/B4)</math></b>	<b>0.001</b>	<b>-0.36</b>	<b>0.061</b>	<b>-0.121</b>	<b>0.825</b>	<b>31.33</b>	<b>&lt;0.001</b>	<b>0.010</b>
	$a_{440} = b_0 \times \ln(B3/B4) + b_1$	-0.027	0.011	—	—	0.625	53.20	<0.001	0.006

K2005 stands for model in [28], G2011 in [57], H2016 in [3], and G2018 in [11].

Due to the frequent cloud cover and longer coverage cycle in Arctic regions, we only obtained 15 sets of quasi-synchronized Sentinel-2 data for Arctic rivers during the ice-free period in this study. To minimize the influence of random factors, we applied a reliable “leave-one-out cross-validation” uncertainty assessment method to calibrate and validate the model. We conducted our modeling using all the paired remote sensing reflectance and CDOM; used one pair of data to validate the models; and calculated the R<sup>2</sup>s, MREs, P-values, and RMSEs. As shown in Table 3, some of the models demonstrated satisfactory results, but the model that was proposed in this study yielded the optimal performance as follows:

$$a_{375} = b_0 + b_1 \times B2 + b_2 \times B2/B4 + b_3 \times \ln(B3/B4), \quad (2)$$

The model displayed both a high explanatory capability and a high predictive power with an R<sup>2</sup> of 0.825, an MRE of 31.33%, and an RMSE of 0.01 m<sup>-1</sup>. Figure 2 demonstrates the correlations between the predicted and measured CDOM ( $a_{375}$ ). The scatters fell evenly on both sides of the 1:1 line, and all the predicted CDOM values were within the field measurement range. The less satisfactory performances of the previous models with our data might be attributed to the differences in the sensor bandwidths, water qualities, and biogeochemical conditions.

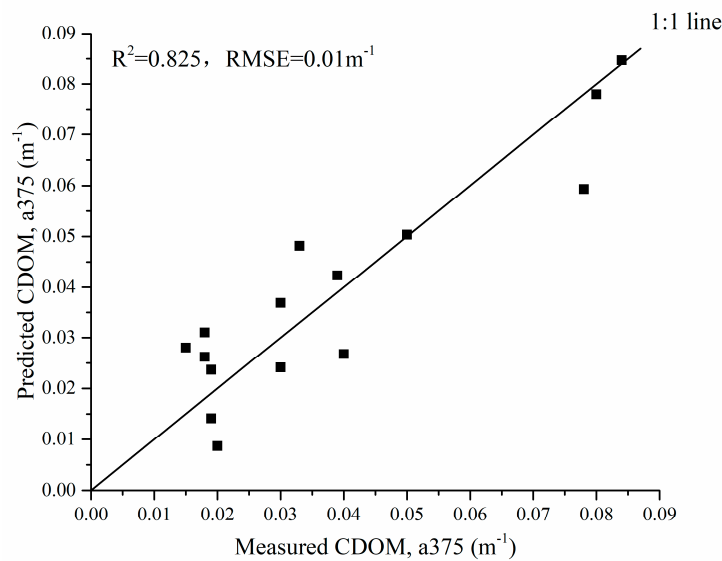


**Figure 2.** Relationship between the measured and predicted CDOM (a375).

### 3. Results

#### 3.1. Correlation between CDOM and DOC in Arctic Rivers

As pointed out by previous studies [21,58], CDOM can be a common and efficient proxy for DOC in many complex waters at high latitudes, including Arctic rivers. In situ data from many different study areas have verified that there are no major outliers affecting the correlations between CDOM and DOC [21,58]. In this study, we divided the field measured CDOM and DOC from the PARTNERS/Arctic-GRO datasets into two parts. The data that were synchronized with the remote sensing images were used as validation data ( $N = 15$ ), and the remaining data were used as training data ( $N = 275$ ) for the ordinary least squares regression. According to our data, the strong correlation between CDOM and DOC ( $R^2 = 0.89$ ) was shown in Figure 3A and expressed by the following formula:

$$\text{DOC} = 129.92 \times \text{CDOM} + 1.81, \quad (3)$$

where DOC is the DOC concentration (mg/L), and CDOM is the absorption coefficient at 375 nm ( $a_{375}, \text{m}^{-1}$ ). The DOC varies from 2.1 to 23.5 mg/L with a mean value of 6.82 mg/L, and the CDOM ranges from 0.004 to 0.129  $\text{m}^{-1}$  with a mean value of 0.039  $\text{m}^{-1}$ . In addition, a strong correlation between CDOM and DOC was also reported in the Kolyma watershed by Griffin et al. [57] ( $R^2 = 0.86$ ,  $N = 54$ ), the Yenisey watershed by Herrault et al. [3] ( $R^2 = 0.84$ ,  $N = 69$ ), and watersheds of the six largest rivers in the Arctic by Griffin et al. [11] ( $R^2 = 0.88$ ,  $N = 248$ ). The strong dependence between the CDOM and DOC revealed in our data and previous studies of Arctic rivers provided strong support for our CDOM-DOC remote sensing retrieval algorithm.

Then, the remote sensing retrieved CDOM from Equation (2) were further converted into DOC concentrations (mg/L) using Equation (3). The relationship between the predicted and measured DOC was plotted in Figure 3B to evaluate the ability of the remote sensing prediction model to estimate the DOC in Arctic rivers. Although the error propagation would lead to higher uncertainties in the predicted DOC than the predicted CDOM, the correlation between the predicted and measured DOC is still very strong ( $R^2 = 0.90$ ,  $P < 0.001$ ,  $\text{RMSE} = 0.842 \text{ mg/L}$ ). Our results confirmed the theory that CDOM has a strong correlation with DOC in Arctic rivers and could be used as an efficient proxy for estimating the DOC discharge into the AO from Arctic rivers [16,21,58].

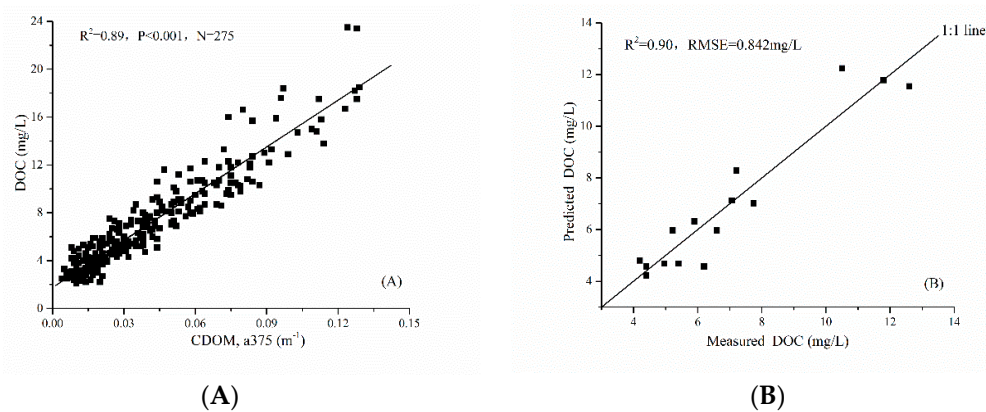


**Figure 3.** (A) Linear regression between the in-situ dissolved organic carbon (DOC) and CDOM (a375), and (B) the relationship between the measured and predicted DOC.

### 3.2. Spatial-Temporal Distribution of DOC

For the results to correspond to distinct hydrologic phases, the DOC concentration of each river was binned into three seasons: spring (May to June), summer (July to October), and winter (November to April) following previous studies [11,49,57]. Although there have been different binning methods for seasonal river discharges across Arctic regions [39,59], our bins captured the characteristics of the seasonal flow transformation. On account of the atrocious weather and longstanding cryoconite cover during winter across the Arctic, it is difficult to acquire valid Sentinel-2 images in the winter. As a result, we could only assess the seasonal variations of the DOC concentrations of Arctic rivers in the spring and summer, and the annual average DOC that is used in this study is the average DOC of the spring and summer of each year.

After validation of the retrieval model for CDOM and DOC, we applied Equations (2) and (3) to all the available Sentinel-2 images of the six largest Arctic rivers from 2016 to 2018 ( $n = 521$ ). The spatial-temporal distributions of the DOC near sampling sites for six largest Arctic rivers are shown in Figure 4, with arrows pointing to the river mouths. The first and second columns are the average DOCs of spring and summer, respectively, and the last column is the annual average DOC. Each row represents the DOC variation for one of the six rivers: Yenisey, Lena, Ob', Kolyma, Yukon, and Mackenzie.

In general, the DOC concentration in spring is obviously greater than that in summer. High DOC concentrations were observed in the spring for the Ob' (Figure 4G) and Lena (Figure 4D), while low DOC concentrations appeared in summer for the Yukon (Figure 4N) and Mackenzie (Figure 4Q). The DOC concentration differences between spring and summer for the Kolyma and Yukon were more obvious than those for the other rivers. In addition, the DOC concentration increases as water flows from tributaries toward the river mouth. The increasing DOC was observed from the midstream to the riverbanks, especially for the Yenisey (Figure 4A–C) and Kolyma (Figure 4J,K,L).

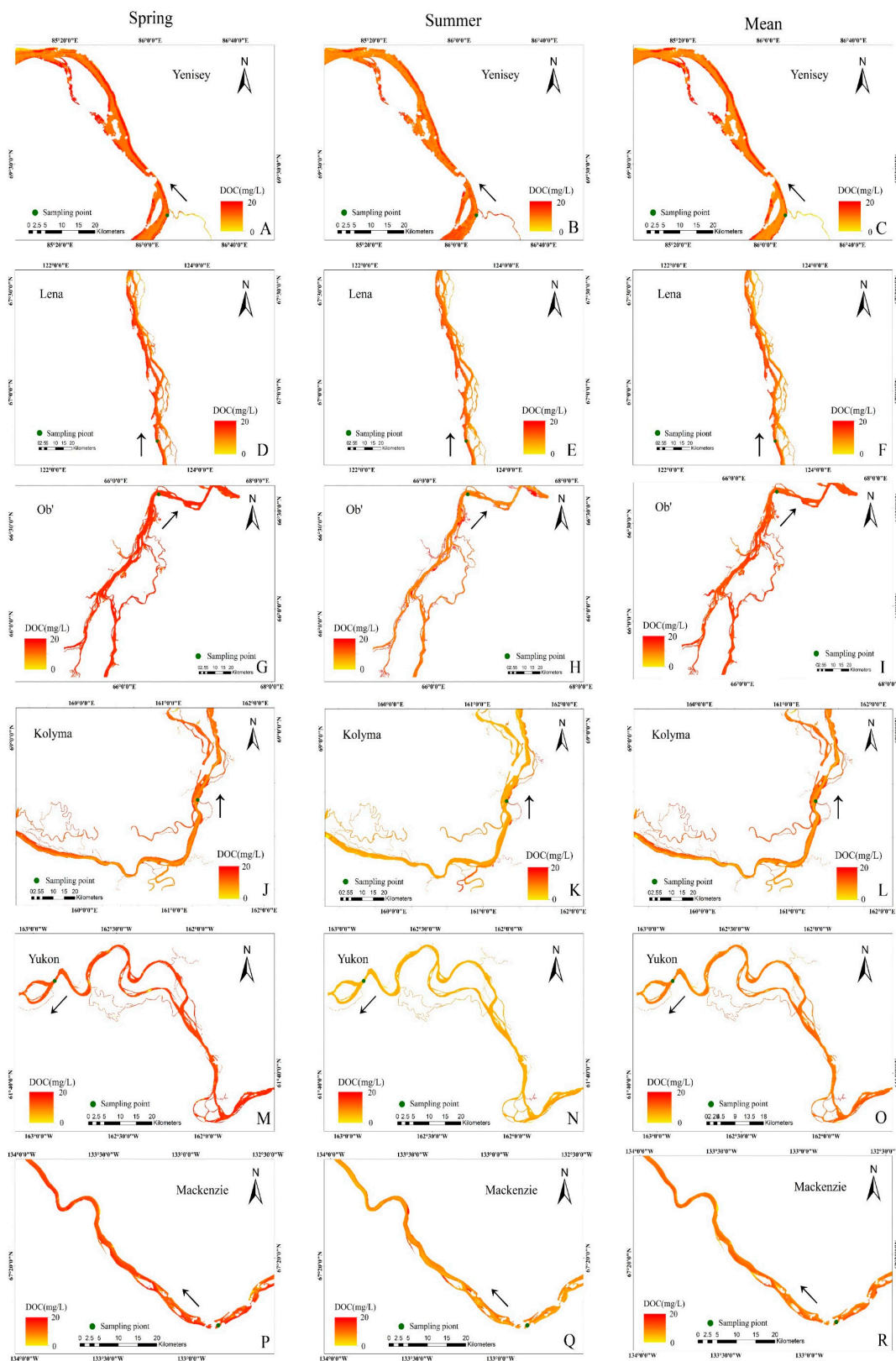


**Figure 4.** Spatial distributions of DOC for the six largest Arctic rivers retrieved from Sentinel-2 images. The arrows point to the river mouths. The first column (A,D,G,J,M,P) is the average DOC for spring, the second column (B,E,H,K,N,Q) is average DOC for summer, and the last column (C,F,I,L,O,R) is the annual average DOC. Each row represents the DOC variation for one of the six rivers: Yenisey, Lena, Ob', Kolyma, Yukon, and Mackenzie.

As the temperature steadily rises from late May to early June in the Arctic, the snow cover starts to melt and the rivers' discharge increases, resulting in a spring freshet every year. The DOC concentration quickly increases as the river discharge increases during the spring freshet. Meanwhile, the DOC concentration remains stable in the following summer months without enough supplement from ice and snow. As shown in Table 4, the DOC in spring is obviously larger than that in summer for all six rivers. The retrieved annual average DOC concentrations decreased in the following order: Ob', Lena, Yenisey, Yukon, Kolyma, and Mackenzie. The Ob' had the largest retrieved DOC (11.00 mg/L) throughout the year, while the Kolyma and Mackenzie had the two smallest DOC concentrations in both seasons. The largest seasonal variation in the DOC (4.08 mg/L) was observed on the Kolyma, and the Mackenzie displayed the smallest concentration difference between spring and summer (1.21 mg/L). The variation ranges and mean values of the remote sensing retrieved DOC for the six rivers in Table 4 are in good agreement with the results in Table 1 and Figure 4.

**Table 4.** Statistics of the retrieved DOC concentrations (mg/L) for six Arctic rivers.

Season		Yenisey	Lena	Ob'	Kolyma	Yukon	Mackenzie
Spring	Min	6.60	9.78	6.94	7.66	7.41	5.46
	Max	24.14	12.48	14.59	11.34	9.92	7.82
	Mean	10.31	11.00	9.93	8.72	8.50	6.46
Summer	Min	4.44	5.99	3.91	2.52	4.97	3.52
	Max	9.55	10.75	7.62	7.14	7.02	6.93
	Mean	6.87	8.90	6.28	4.64	5.83	5.25
Annual Average		7.50	9.02	9.45	6.05	6.61	5.75

#### 4. Discussion

The DOC concentration varies greatly in Arctic regions. DOC transportation from land to ocean through river systems is mainly influenced by natural and artificial processes. Many factors, such as the topography, hydrology, soil, land cover, eutrophication, and human activities, play critical roles in regulating the DOC concentration in water bodies [38,47,60]. To obtain a better understanding of the role of DOC in the ecological environment, we quantitatively analyzed the effects of different potential drivers on the DOC concentration using field measured data and remote sensing data.

##### 4.1. Natural Influence Factors

The Arctic rivers carry large amounts of DOC into the AO, which mainly occurs through river discharge [11,61]. Thanks to the abundant field-measured data at river mouths from the Arctic-GRO and PARTNERS projects, we were able to analyze the correlations between the river discharges of the six largest Arctic rivers and the corresponding DOC concentrations from 2016 to 2018 ( $n = 136$ ). As shown in Figure 5, a positive correlation was found for all six watersheds ( $R^2 = 0.54$ ,  $P < 0.001$ ). The peak values of the DOC concentrations and river discharges are quasi-synchronously observed in the spring (our data and figure can be found in the Supplementary Materials). This phenomenon was also reported in previous studies on the dynamic variation of riverine DOC in the Arctic and other rivers in high latitude areas [2,43,62,63]. Previous studies pointed out that the river discharge, as a primary carrier of DOC, was a critical means of DOC transportation [13,16,24,60]. The surge of precipitation and extensive snowmelt generate unique spring freshets across Arctic regions. The organic carbon in the topsoil is moved by rainfall and melting water into rivers, leading to a rapid increase in river discharge and DOC concentration. In comparison, snowmelt and precipitation decrease in summer, resulting in the deeper infiltration of solutions into the soil [64,65]. Consequently, the humid environment caused by warming weather and the extension of the stay time of the DOC in the soil could accelerate the microbial mineralization process and decrease the output of terrestrial organic carbon in the river system. The low DOC concentration would continue through summer and winter.

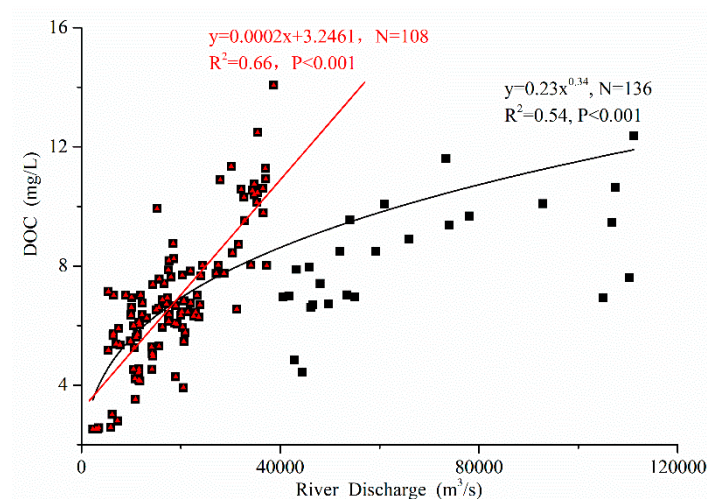


**Figure 5.** Correlations between the DOC concentration and river discharge. The black squares and black line represent all available data, and the red triangles and red line represent the data with discharges less than 40,000 m<sup>3</sup>/s.

Further analysis revealed that, if the dataset was divided into two parts according to discharge, the data with discharge less than 40,000 m<sup>3</sup>/s could display a stronger correlation ( $R^2 = 0.66$ ,  $P < 0.001$ , red triangles in Figure 5). In addition, more than 70% of the data with small discharge were measured in summer. This result indicated that the unique and drastic spring freshet might raise the uncertainty of the correlation between the discharge and DOC. However, compared to the strong correlations that were reported in [11,61,65], the river discharge only explained 54% of the variation in the DOC in our study. Therefore, we should carefully consider more factors.

According to previous studies [38,39,47], the watershed slope is a promising indicator of the DOC variation in rivers. To analyze the similarities and differences for the six rivers, we calculated the mean slopes of 35 sub-catchments in Arctic regions, as described in Section 2.3, and quantified the correlation between the watershed slopes and the DOC concentration. As shown in Figure 6, there is a weak negative correlation between the DOC and the watershed slopes of all 35 sub-catchments ( $R^2 = 0.35$ ,  $P < 0.001$ ), indicating that gentler slopes result in high DOC concentrations and steeper slopes result in low DOC concentrations. Since the study area in this paper ( $\sim 20.5 \times 10^6$  km<sup>2</sup>) is much larger than those in previous studies, the differences in the topographic features and geographical variations might introduce more uncertainties to our results.

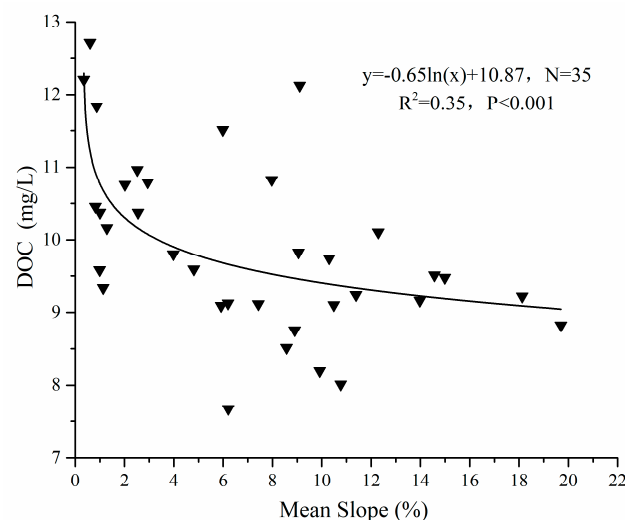


**Figure 6.** Correlation between the watershed slope and DOC concentration.

To further analyze the characteristics of the correlation between the DOC and watershed slopes, we divided the 35 sub-catchments into two groups according to their geographical position and watershed area, respectively. According to first classification method, the Eurasian rivers (including the drainage basins of the Yenisey, Lena, Ob', and Kolyma) demonstrated a stronger negative correlation ( $R^2 = 0.48$ ,  $N = 22$ ) than that of the North American rivers (including the drainage basins of the Yukon and Mackenzie, with  $R^2 = 0.14$  and  $N = 13$ ). Further analysis revealed that the West Siberian Plain (including the Yenisey and Ob' drainage basins) and the East Siberian Mountains (the Kolyma drainage basin) both had strong negative correlations between the watershed slope and the DOC, with  $R^2$ s reaching up to 0.78 ( $N = 9$ ) and 0.89 ( $N = 6$ ), respectively. In comparison, the correlation for the central Siberian Plateau (Lena drainage basin) was relatively weak ( $R^2 = 0.47$ ,  $N = 7$ ).

Steep slopes are usually accompanied by deeper vertical permeability and greater influence from underground water [66,67]. For permafrost regions, however, tundra could serve as an impermeable barrier and prevent water from penetrating deeper into the soil [68]. Due to limited vertical drainage, melting water was detained in surface soil, and absorbed or degraded by organic matter in soil, leading to a decrease in DOC concentration [39,60,68–70]. In comparison, gentle slopes could facilitate the near surface flow path and augment the contact area and time between water and soil that is rich in organic matter, which would accelerate the humification of macromolecular organic matter and increase the DOC concentration [38,39,46,71,72]. This could explain why steep slopes are accompanied by low DOC concentrations and vice versa for most Eurasian watersheds in the Arctic. For another, the North American rivers in the Arctic (the Yukon and Mackenzie) are characterized by complicated terrain with unconsolidated sediments and consolidated rocks [17]. During spring floods, the melting ice carries large amounts of suspended sediment into rivers, thus leading to sudden rises in the TSS, as displayed in Table 2. The potential role of the highly concentrated sediment in adsorbing the DOM in water, as reported by Amon et al. [17], might account for the low DOC in these rivers. In addition, the lakes and wetlands along the rivers might change the proportion of DOM that is transported along the riverbanks [73]. As pointed out by Yi et al. [74], the Great Slave Lake contributes 55.7% of its water composition to the main flow of the Mackenzie River. The buffering capacity of open waters could increase the dwell time of the DOM and the uncertainty of the DOC variation.

According to the second classification method, the watershed slopes of small (<60,000 km<sup>2</sup>) and moderate (60,000–150,000 km<sup>2</sup>) drainage basins, respectively, explained 69% ( $N = 9$ ) and 34% ( $N = 15$ ) of the variability in DOC, while only 14% ( $N = 11$ ) of the variability in the DOC could be attributed to the watershed slopes of large drainage basins (>150,000 km<sup>2</sup>) in Figure 7. The small drainage basins usually possess relatively analogical geomorphic features and hydrologic conditions, leading to a better explanatory ability for the slope-concentration relationships of the DOC. In comparison, the large drainage basins might be influenced by many factors, and large-amplitude variations may cause uncertainties. However, the scale-dependent effects on the slope-concentration relationships for the DOC that are reported here still need additional data to corroborate them. As a result, the correlation between the DOC and watershed slopes was not only geographic-dependent but also scale-dependent.

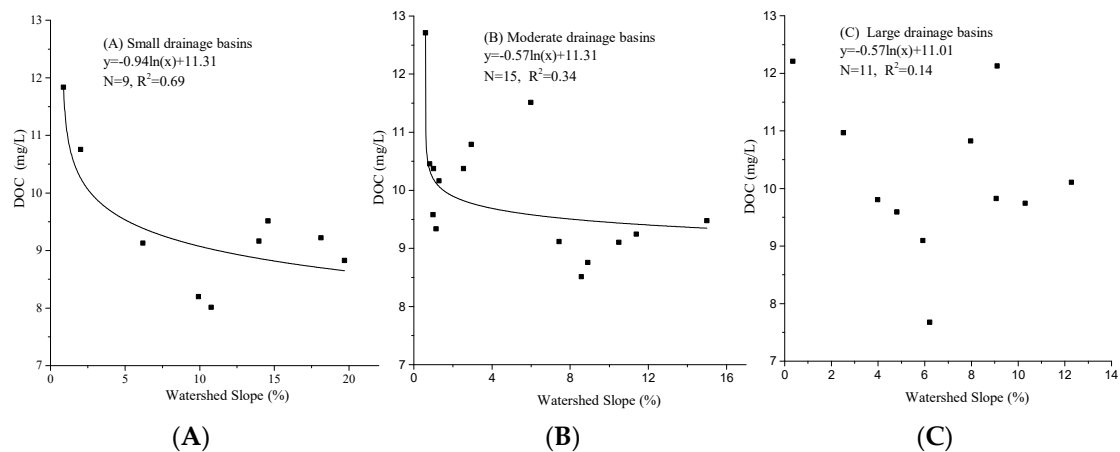


**Figure 7.** Correlation between the watershed slope and DOC concentration for (A) small, (B) moderate, and (C) large drainage basins.

#### 4.2. Artificial Influence Factors

Human activities, such as the destruction of shrubs and vegetation, infrastructure construction, changes in cultivation modes, and rapid urbanization, would interfere with natural processes and the output environment of organic matter in watersheds [75]. As shown by the spatial distribution of the DOC in Arctic rivers (Figure 4), the DOC concentration was higher near riverbanks with cities or villages than midstream, indicating a possible influence of artificial factors on the DOC variation.

The human population density (people/km<sup>2</sup>) of each sub-catchment was calculated from LandScan™ 2017 datasets and validated by data from the Arctic-GRO and PARTNERS projects. Then we compared the human population density with the annual average DOC concentration that was retrieved using the remote sensing data in Figure 8. The significantly positive correlation for six rivers ( $R^2 = 0.70$ ,  $P < 0.05$ ) implied anthropogenic interference. The Ob' river has the flattest terrain and the mildest climate among the six Arctic rivers, resulting in the least permafrost. The basin is densely populated, with about 28 million people living on both sides of the river and population density of 9.67 people/km<sup>2</sup>, which is much more than other watersheds in the Arctic [17,41]. In comparison, the watershed of the Kolyma is characterized by an adverse climate and extensive continuous permafrost, with a population density of 0.03 people km<sup>-2</sup> and the second-lowest DOC concentration. According to our data, the human population could affect the DOC concentration to a certain degree, but more influence factors should be taken into consideration.

The main source of DOC in Arctic regions is allochthonous wetlands and forest in terrestrial environments [31]. Previous studies utilized the field-measured forest coverage and wetland area to study the correlation between the DOC and land cover and obtained high accuracies for small-scale study areas [38,47]. The study of Prokushkin et al. [76] confirmed that DOC of Yenisey and its tributaries was mainly derived from the forest of the central Siberian plateau. To sum up, the LUCC not only plays an important role in DOC export but also influences DOC quality through various biogeochemical and biodegradation processes [15].

The high spatial resolution of remote sensing images makes large scale investigations possible and economical. To quantitatively analyze the influence of the land cover on the DOC concentration, we used the Finer Resolution Observation and Monitoring of Global Land Cover datasets that had a 10 m resolution (FROM-GLC10). As described in Section 2.2, there are 10 different land cover types in the FROM-GLC10 datasets and 35 sub-catchments in our study. We first statistically analyzed the proportions of the land cover types in each sub-catchment, and then a correlation analysis was conducted between the annual average DOC concentration and the land cover types.

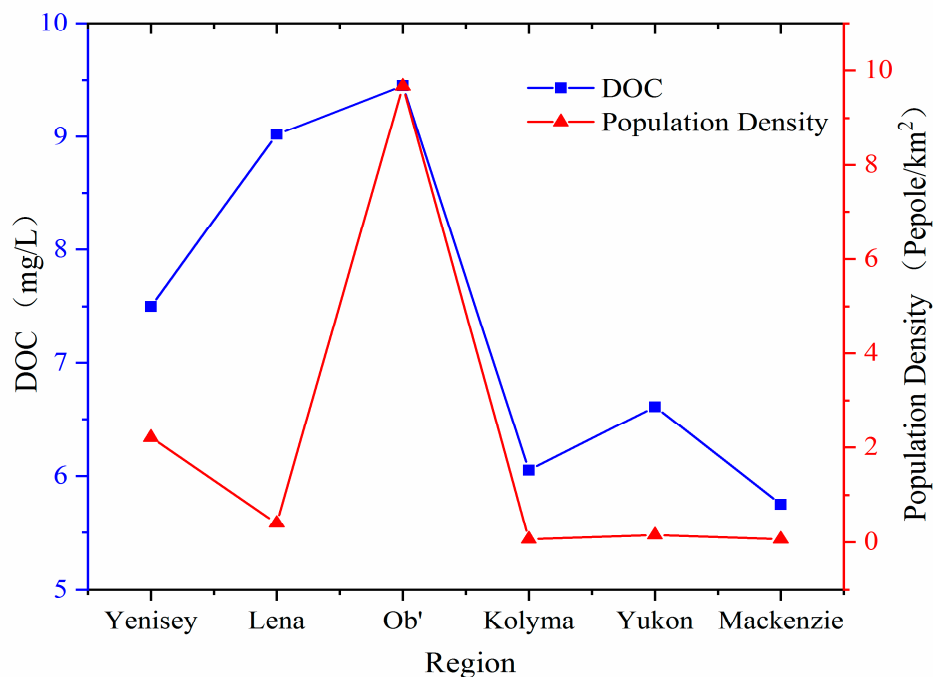


**Figure 8.** Comparison of the human population density with the annual average DOC concentration in the six watersheds.

A stronger positive correlation was found between forest cover and DOC in Figure 9A ( $R^2$  of 0.62,  $P < 0.001$ ), thus providing proof that it is the main source of DOC in Arctic regions. Similar results were reported by Meyer et al. [77], who found that the output of organic carbon decreased after cutting down a forest in the Coweeta watershed. The forest cover explained 62% of the variability in the DOC in our study, indicating that other environmental elements also influenced the organic carbon output of watersheds, such as the topography and hydrology [46,78].

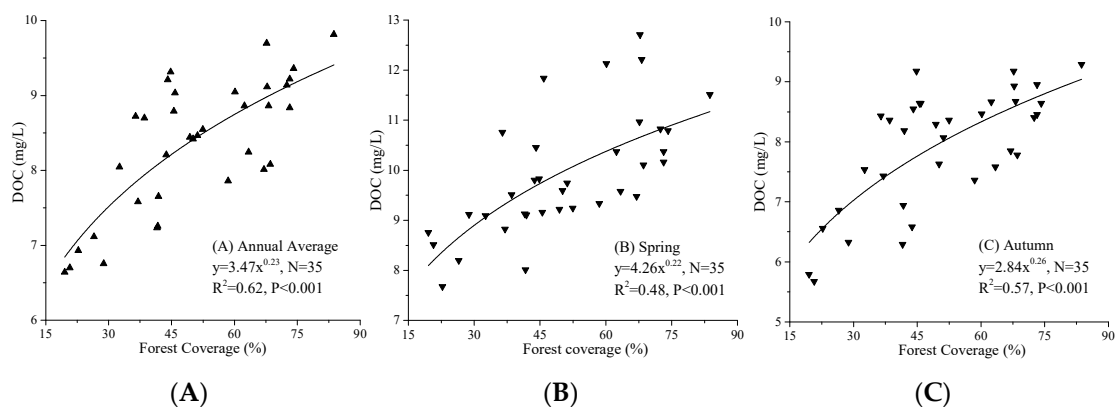


**Figure 9.** Correlation between forest coverage and the DOC concentration: (A) annual average, (B) spring, and (C) summer.

Due to the impermeability of the permafrost that covers most of the Arctic regions, the fluidity of the melting snow and precipitation were confined to the topsoil [68]. Meanwhile, the forest cover and leaf-litter also accumulated on the topsoil and decomposed with the help of microorganisms, forming lignocellulose and humic acid that permeated into the soil. As we discussed in Section 4.1, the spring freshet that is caused by the increased precipitation and snowmelt resulted in the peak DOC concentrations in Arctic rivers. To evaluate the impact of the spring freshet, we compared the correlation between forest cover and the DOC in the spring and summer. As shown in Figure 9B,C, a

stronger correlation was found between the LUCC and DOC in the summer ( $R^2$  of 0.57 and  $P < 0.001$ ) when the influence of the spring freshet was more diminished than in the spring ( $R^2$  of 0.48 and  $P < 0.001$ ). Our findings indicated that the unique and drastic spring freshet might raise the uncertainty of the correlation between the DOC and LUCC.

In order to further analyze the DOM characteristics, such as molecular weight, composition, and age,  $SUVA_{254}$  was calculated, as described in Section 2.1. According to previous studies [21,22,38,50],  $SUVA_{254}$  values are positively correlated with the percent aromaticity and molecular size of DOM. As shown in Table 1, the  $SUVA_{254}$  in Ob' was the largest ( $3.301 \text{ L mg C}^{-1} \text{ m}^{-1}$ ), followed by that in Lena and Yenisey. In comparison, the  $SUVA_{254}$  from Kolyma and Mackenzie were the smallest two. Our results indicated that  $SUVA_{254}$  was a statistically significant predictor of DOC concentration (Table 1). Considering the Ob' contains the largest peat bog system on the planet [17,18] and the largest proportion of wetland among the six Arctic rivers, marsh swamp could be the reason for the high concentration of DOC and  $SUVA_{254}$ .

As a complex ecosystem like the Arctic, the controlling factors of the DOC flux are definitely more than river discharge, watershed slopes, human activities, and the LUCC factors that were discussed in our paper. The increasing river discharge caused by climate change might also contribute to the DOC rise in rivers [41,43]. In addition, massive melting of permafrost, construction of dams, frequent forest fires [42], latitude [79], and concentration and composition of suspended sediment [17] were also considered as important potential influence factors. As a result, more studies are needed to further explore the mechanism of DOC concentration change and the carbon cycle in the Arctic region.

## 5. Conclusions

It is of great importance to advance our understanding of the global carbon cycle using remote sensing algorithms for Arctic rivers. With the help of field-measured data and Sentinel-2 remote sensing data, we developed and validated a CDOM/DOC retrieval algorithm. Then, we obtained the spatial distributions of the DOC in watersheds of the six largest Arctic rivers and 35 sub-catchments between 2016 and 2018. The spatial distribution of DOC showed significant differences in spring and summer. The spring freshet increased river discharge and DOC concentration synchronously, while the river discharge and DOC experienced a steady decline in summer. Our analysis showed that the river discharge, watershed slopes, human activities, and the LUCC were important influence factors of DOC concentrations in rivers across the Pan-Arctic domain. In addition, the seasonality, geography, and scale would affect the correlation between DOC concentration and these influence factors. The first usage of LUCC data with high spatial resolution (10 m) made a quantitative analysis of the correlation between LUCC and DOC concentration possible. According to our data, the forest coverage seemed to play an important role in regulating the DOC flux in the Arctic rivers. More studies are still needed to comprehensively describe the DOC variation in high latitudes regions.

This paper verifies the ability of the remote sensing retrieval algorithm to monitor DOC variations in Arctic rivers during the open-water season. The proposed algorithm is the first attempt to monitor CDOM/DOC variation in the Arctic rivers using high spatiotemporal resolution optical Sentinel-2 data. The satisfying performance ( $R^2 = 0.825$ ,  $RMSE = 0.010 \text{ m}^{-1}$ ) proves that Sentinel-2 offers improved sensitivity for estimating water quality parameters with an improved spatial resolution, better band placement, and increased observation frequency. Our results reveal the successful application of wavelength combinations of Sentinel-2 data to retrieve the CDOM/DOC in high latitude areas. Given that the Arctic environment is rapidly changing, the algorithm that is proposed here might not be able to be reliably applied to future scenarios. This method does, however, provide a basis for the near-term estimation of DOC concentrations and an opportunity for longer-term assessments of the integrated changes in watershed biogeochemistry. Our results could provide a comprehensive evaluation method for riverine DOC in Pan-Arctic regions with remote sensing data.

**Author Contributions:** Conceptualization, J.H.; methodology, J.H. and M.W.; software, M.W.; validation, J.H. and M.W.; formal analysis, J.H.; data curation, M.W.; writing—original draft preparation, J.H.; writing—review and editing, J.H., T.C. and F.Y.; visualization, M.W.; supervision, T.C. and F.Y.; and funding acquisition, T.C.

**Funding:** This study is funded by the National Key Research and Development Program, China (No. 2018YFC1407200), the National Natural Science Foundation of China (Nos. 41706194, 41876206, and 61890964), the Shandong Provincial Natural Science Foundation, China (No. ZR2016DB23), the Scientific Research Foundation of Shandong University of Science and Technology for Recruited Talents (2017RCJJ073), and SDUST Research Fund (2019TDJH103).

**Conflicts of Interest:** The authors declare no conflict of interest.

## References

1. Le Fouest, V.; Matsuoka, A.; Manizza, M.; Shernetsky, M.; Tremblay, B.; Babin, M. Towards an assessment of riverine dissolved organic carbon in surface waters of the western Arctic Ocean based on remote sensing and biogeochemical modeling. *Biogeosciences* **2018**, *15*, 1335–1346. [CrossRef]
2. Holmes, R.M.; McClelland, J.W.; Peterson, B.J.; Tank, S.E.; Bulygina, E.; Eglinton, T.I.; Gordeev, V.V.; Gurtovaya, T.Y.; Raymond, P.A.; Repeta, D.J.; et al. Seasonal and annual fluxes of nutrients and organic matter from large rivers to the arctic ocean and surrounding seas. *Estuaries Coasts* **2011**, *35*, 369–382. [CrossRef]
3. Herrault, P.A.; Gandois, L.; Gascoin, S.; Tananaev, N.; Le Dantec, T.; Teisserenc, R. Using high spatio-temporal optical remote sensing to monitor dissolved organic carbon in the arctic river yenisei. *Remote Sens.* **2016**, *8*, 803. [CrossRef]
4. Brown, R.; Derksen, C.; Wang, L. A multi-data set analysis of variability and change in Arctic spring snow cover extent 1967–2008. *J. Geophys. Res. Atmos.* **2010**, *115*, D16111. [CrossRef]
5. Romanovsky, V.E.; Smith, S.L.; Christiansen, H.H. Permafrost thermal state in the polar Northern Hemisphere during the international polar year 2007–2009: A synthesis. *Permafrost. Periglac. Process.* **2010**, *21*, 106–116. [CrossRef]
6. Vonk, J.E.; Tank, S.E.; Bowden, W.B.; Laurion, I.; Vincent, W.F.; Alekseychik, P.; Amyot, M.; Billett, M.; Canario, J.; Cory, R.M. Reviews and syntheses: Effects of permafrost thaw on Arctic aquatic ecosystems. *Biogeosciences* **2015**, *12*, 7129–7167. [CrossRef]
7. Tarnocai, C.; Canadell, J.G.; Schuur, E.A.G.; Kuhry, P.; Mazhitova, G.; Zimov, S. Soil organic carbon pools in the northern circumpolar permafrost region. *Glob. Biogeochem. Cycles* **2009**, *23*, GB003327. [CrossRef]
8. Tank, S.E.; Raymond, P.A.; Striegl, R.G.; McClelland, J.W.; Holmes, R.M.; Fiske, G.J.; Peterson, B.J. A land-to-ocean perspective on the magnitude, source and implication of DIC flux from major Arctic rivers to the Arctic Ocean. *Glob. Biogeochem. Cycles* **2012**, *26*, GB4018. [CrossRef]
9. Holmes, R.M.; McClelland, J.W.; Tank, S.E.; Spencer, R.G.M.; Shiklomanov, A.I. Arctic Great Rivers Observatory. Water Quality Dataset, Version 20181010. 2018. Available online: <https://www.arcticgreatrivers.org/data> (accessed on 23 June 2019).
10. Shiklomanov, A.I.; Holmes, R.M.; McClelland, J.W.; Tank, S.E.; Spencer, R.G.M. Arctic Great Rivers Observatory. Discharge Dataset, Version 20190618. 2018. Available online: <https://www.arcticgreatrivers.org/data> (accessed on 24 June 2019).
11. Griffin, C.G.; McClelland, J.W.; Frey, K.E.; Fiske, G.; Holmes, R.M. Quantifying CDOM and DOC in major Arctic rivers during ice-free conditions using Landsat TM and ETM+ data. *Remote Sens. Environ.* **2018**, *209*, 395–409. [CrossRef]
12. Tank, S.E.; Striegl, R.G.; McClelland, J.W.; Kokelj, S.V. Multi-decadal increases in dissolved organic carbon and alkalinity flux from the Mackenzie drainage basin to the Arctic Ocean. *Environ. Res. Lett.* **2016**, *11*, 054015. [CrossRef]
13. McClelland, J.W.; Holmes, R.M.; Peterson, B.J.; Raymond, P.A.; Striegl, R.G.; Zhulidov, A.V.; Zimov, S.A.; Zimov, N.; Tank, S.E.; Spencer, R.G.M.; et al. Particulate organic carbon and nitrogen export from major Arctic rivers. *Glob. Biogeochem. Cycles* **2016**, *30*, 629–643. [CrossRef]
14. Cole, J.J.; Prairie, Y.T.; Caraco, N.F.; McDowell, W.H.; Tranvik, L.J.; Striegl, R.G.; Duarte, C.M.; Kortelainen, P.; Downing, J.A.; Middelburg, J.J.; et al. Plumbing the global carbon cycle: Integrating inland waters into the terrestrial carbon budget. *Ecosystems* **2007**, *10*, 172–185. [CrossRef]

15. Singh, S.; Dash, P.; Silwal, S.; Feng, G.; Adeli, A.; Moorhead, R.J. Influence of land use and land cover on the spatial variability of dissolved organic matter in multiple aquatic environments. *Environ. Sci. Pollut. Res. Int.* **2017**, *24*, 14124–14141. [[CrossRef](#)] [[PubMed](#)]
16. Stedmon, C.A.; Amon, R.M.W.; Rinehart, A.J.; Walker, S.A. The supply and characteristics of colored dissolved organic matter (CDOM) in the Arctic Ocean: Pan Arctic trends and differences. *Mar. Chem.* **2011**, *124*, 108–118. [[CrossRef](#)]
17. Amon, R.M.W.; Rinehart, A.J.; Duan, S.; Louchouart, P.; Prokushkin, A.; Guggenberger, G.; Bauch, D.; Stedmon, C.; Raymond, P.A.; Holmes, R.M.; et al. Dissolved organic matter sources in large Arctic rivers. *Geochim. Cosmochim. Acta* **2012**, *94*, 217–237. [[CrossRef](#)]
18. Kaiser, K.; Canedo-Oropeza, M.; McMahon, R.; Amon, R.M.W. Origins and transformations of dissolved organic matter in large Arctic rivers. *Sci. Rep.* **2017**, *7*, 13064. [[CrossRef](#)]
19. Ylöstalo, P.; Kallio, K.; Seppälä, J. Absorption properties of in-water constituents and their variation among various lake types in the boreal region. *Remote Sens. Environ.* **2014**, *148*, 190–205. [[CrossRef](#)]
20. Hugelius, G.; Strauss, J.; Zubrzycki, S.; Harden, J.W.; Schuur, E.A.G.; Ping, C.L.; Schirmer, L.; Grosse, G.; Michaelson, G.J.; Koven, C.D.; et al. Estimated stocks of circumpolar permafrost carbon with quantified uncertainty ranges and identified data gaps. *Biogeosciences* **2014**, *11*, 6573–6593. [[CrossRef](#)]
21. Frey, K.E.; Sobczak, W.V.; Mann, P.J.; Holmes, R.M. Optical properties and bioavailability of dissolved organic matter along a flow-path continuum from soil pore waters to the Kolyma River mainstem, East Siberia. *Biogeosciences* **2016**, *13*, 2279–2290. [[CrossRef](#)]
22. O'Donnell, J.A.; Aiken, G.R.; Swanson, D.K.; Panda, S.; Butler, K.D.; Baltensperger, A.P. Dissolved organic matter composition of Arctic rivers: Linking permafrost and parent material to riverine carbon. *Glob. Biogeochem. Cycles* **2016**, *30*, 1811–1826. [[CrossRef](#)]
23. Spencer, R.G.M.; Butler, K.D.; Aiken, G.R. Dissolved organic carbon and chromophoric dissolved organic matter properties of rivers in the USA. *J. Geophys. Res. Biogeosci.* **2012**, *117*, G03001. [[CrossRef](#)]
24. Del Castillo, C.E.; Miller, R.L. On the use of ocean color remote sensing to measure the transport of dissolved organic carbon by the Mississippi River Plume. *Remote Sens. Environ.* **2008**, *112*, 836–844. [[CrossRef](#)]
25. Matsuoka, A.; Babin, M.; Doxaran, D.; Hooker, S.B.; Mitchell, B.G.; Bélanger, S.; Bricaud, A. A synthesis of light absorption properties of the Arctic Ocean: Application to semi-analytical estimates of dissolved organic carbon concentrations from space. *Biogeosciences* **2014**, *11*, 3131–3147. [[CrossRef](#)]
26. Strömbeck, N.; Pierson, D.C. The effects of variability in the inherent optical properties on estimations of chlorophyll a by remote sensing in Swedish freshwaters. *Sci. Total Environ.* **2001**, *268*, 123–137. [[CrossRef](#)]
27. Brezonik, P.; Menken, K.D.; Bauer, M. Landsat-based remote sensing of lake water quality characteristics, including chlorophyll and Colored Dissolved Organic Matter (CDOM). *Lake Reserv. Manag.* **2005**, *21*, 373–382. [[CrossRef](#)]
28. Kutser, T.; Pierson, D.C.; Kallio, K.Y.; Reinart, A.; Sobek, S. Mapping lake CDOM by satellite remote sensing. *Remote Sens. Environ.* **2005**, *94*, 535–540. [[CrossRef](#)]
29. Zhu, W.; Yu, Q.; Tian, Y.Q.; Chen, R.F.; Gardner, G.B. Estimation of chromophoric dissolved organic matter in the Mississippi and Atchafalaya river plume regions using above-surface hyperspectral remote sensing. *J. Geophys. Res.* **2011**, *116*, C02011. [[CrossRef](#)]
30. Tian, Y.Q.; Yu, Q.; Zhu, W. Estimating of chromophoric dissolved organic matter (CDOM) with in-situ and satellite hyperspectral remote sensing technology. In Proceedings of the 2012 IEEE International Geoscience and Remote Sensing Symposium, Munich, Germany, 22–27 July 2012; pp. 2040–2042.
31. Brezonik, P.L.; Olmanson, L.G.; Finlay, J.C.; Bauer, M.E. Factors affecting the measurement of CDOM by remote sensing of optically complex inland waters. *Remote Sens. Environ.* **2015**, *157*, 199–215. [[CrossRef](#)]
32. Kutser, T. The possibility of using the Landsat image archive for monitoring long time trends in coloured dissolved organic matter concentration in lake waters. *Remote Sens. Environ.* **2012**, *123*, 334–338. [[CrossRef](#)]
33. Fichot, C.G.; Kaiser, K.; Hooker, S.B.; Amon, R.M.W.; Babin, M.; Bélanger, S.; Walker, S.A.; Benner, R. Pan-Arctic distributions of continental runoff in the Arctic Ocean. *Sci. Rep.* **2013**, *3*, 1–6. [[CrossRef](#)]
34. Zhu, W.; Yu, Q.; Tian, Y.Q.; Becker, B.L.; Zheng, T.; Carrick, H.J. An assessment of remote sensing algorithms for colored dissolved organic matter in complex freshwater environments. *Remote Sens. Environ.* **2014**, *140*, 766–778. [[CrossRef](#)]

35. Huang, L.; Zheng, Y.; Yu, Q.; Tian, Y.Q.; Zhu, W.; Chen, J. Remote estimation of colored dissolved organic matter and chlorophyll-a in Lake Huron using Sentinel-2 measurements. *J. Appl. Remote Sens.* **2017**, *11*, 036007.
36. Pelevin, V.V.; Zavjalov, P.O.; Belyaev, N.A.; Konovalov, B.V.; Kravchishina, M.D.; Mosharov, S.A. Spatial variability of concentrations of chlorophyll a, dissolved organic matter and suspended particles in the surface layer of the kara sea in september 2011 from lidar data. *Oceanology* **2017**, *57*, 165–173. [[CrossRef](#)]
37. Belen Ruescas, A.; Hieronymi, M.; Mateo-Garcia, G.; Koponen, S.; Kallio, K.; Camps-Valls, G. Machine learning regression approaches for Colored Dissolved Organic Matter (CDOM) retrieval with S2-MSI and S3-OLCI simulated data. *Remote Sens.* **2018**, *10*, 786. [[CrossRef](#)]
38. Harms, T.K.; Edmonds, J.W.; Genet, H.; Creed, I.F.; Aldred, D.; Balser, A.; Jones, J.B. Catchment influence on nitrate and dissolved organic matter in Alaskan streams across a latitudinal gradient. *J. Geophys. Res. Biogeosci.* **2016**, *121*, 350–369. [[CrossRef](#)]
39. Connolly, C.T.; Khosh, M.S.; Burkart, G.A.; Douglas, T.A.; Holmes, R.M.; Jacobson, A.D.; Tank, S.E.; McClelland, J.W. Watershed slope as a predictor of fluvial dissolved organic matter and nitrate concentrations across geographical space and catchment size in the Arctic. *Environ. Res. Lett.* **2018**, *13*, 104015. [[CrossRef](#)]
40. Serreze, M.C.; Bromwich, D.H.; Clark, M.P.; Etringer, A.J.; Zhang, T.; Lammers, R. Large-scale hydro-climatology of the terrestrial Arctic drainage system. *J. Geophys. Res.* **2002**, *108*, 8106. [[CrossRef](#)]
41. Yang, D.; Ye, B.; Shiklomanov, A. Discharge Characteristics and Changes over the Ob River Watershed in Siberia. *J. Hydrometeorol.* **2004**, *5*, 595–610. [[CrossRef](#)]
42. McClelland, J.W. Increasing river discharge in the Eurasian Arctic: Consideration of dams, permafrost thaw, and fires as potential agents of change. *J. Geophys. Res.* **2004**, *109*, D18102. [[CrossRef](#)]
43. Raymond, P.A.; McClelland, J.W.; Holmes, R.M.; Zhulidov, A.V.; Mull, K.; Peterson, B.J.; Striegl, R.G.; Aiken, G.R.; Gurtovaya, T.Y. Flux and age of dissolved organic carbon exported to the Arctic Ocean: A carbon isotopic study of the five largest arctic rivers. *Glob. Biogeochem. Cycles* **2007**, *21*, GB4011. [[CrossRef](#)]
44. Schiff, S.L.; Devito, K.J.; Elgood, R.J.; McCrindle, P.M.; Spoelstra, J.; Dillon, P. Two adjacent forested catchments: Dramatically different NO<sub>3</sub>–export. *Water Resour. Res.* **2002**, *38*, 1292. [[CrossRef](#)]
45. Inamdar, S.P.; Mitchell, M.J. Hydrologic and topographic controls on storm-event exports of dissolved organic carbon (DOC) and nitrate across catchment scales. *Water Resour. Res.* **2006**, *42*, W03421. [[CrossRef](#)]
46. Winn, N.; Williamson, C.E.; Abbitt, R.; Rose, K.; Renwick, W.; Henry, M.; Saros, J. Modeling dissolved organic carbon in subalpine and alpine lakes with GIS and remote sensing. *Landsc. Ecol.* **2009**, *24*, 807–816. [[CrossRef](#)]
47. D’Amore, D.V.; Edwards, R.T.; Biles, F.E. Biophysical controls on dissolved organic carbon concentrations of Alaskan coastal temperate rainforest streams. *Aquat. Sci.* **2015**, *78*, 381–393. [[CrossRef](#)]
48. Walker, S.A.; Amon, R.M.W.; Stedmon, C.A. Variations in high-latitude riverine fluorescent dissolved organic matter: A comparison of large Arctic rivers. *J. Geophys. Res. Biogeosci.* **2013**, *118*, 1689–1702. [[CrossRef](#)]
49. Holmes, R.M.; Coe, M.; Fiske, G.; Gurtovaya, T.; McClelland, J.; Shiklomanov, A.; Spencer, R.; Tank, S.; Zhulidov, A. *Climate Change Impacts on the Hydrology and Biogeochemistry of Arctic Rivers, in Global Impacts of Climate Change on Inland Waters*; John Wiley & Sons, Ltd: Hoboken, NJ, USA, 2013; pp. 3–26.
50. Weishaar, J.L.; Aiken, G.R.; Bergamaschi, B.A.; Fram, M.S.; Fujii, R.; Mopper, K. Evaluation of specific ultraviolet absorbance as an indicator of the chemical composition and reactivity of dissolved organic carbon. *Environ. Sci. Technol.* **2003**, *37*, 4702–4708. [[CrossRef](#)]
51. The ArcticRIMS Website. Available online: <http://rims.unh.edu/data.shtml> (accessed on 13 June 2019).
52. FROM-GLC (Finer Resolution Observation and Monitoring of Global Land Cover). Available online: <http://data.ess.tsinghua.edu.cn> (accessed on 16 August 2019).
53. Gong, P.; Liu, H.; Zhang, M.; Li, C.; Wang, J.; Huang, H.; Clinton, N.; Ji, L.; Li, W.; Bai, Y.; et al. Stable classification with limited sample: Transferring a 30-m resolution sample set collected in 2015 to mapping 10-m resolution global land cover in 2017. *Sci. Bull.* **2019**, *64*, 370–373. [[CrossRef](#)]
54. GMTED2010 DEM Data. Available online: <https://earthexplorer.usgs.gov/> (accessed on 8 July 2019).
55. ORNL’s LandScan™ 2017 Datasets. Available online: <https://landscan.ornl.gov/landscan-datasets> (accessed on 14 November 2019).
56. Joshi, I.; D’Sa, E. Seasonal variation of colored dissolved organic matter in barataria bay, louisiana, using combined landsat and field data. *Remote Sens.* **2015**, *7*, 12478–12502. [[CrossRef](#)]

57. Griffin, C.G.; Frey, K.E.; Rogan, J.; Holmes, R.M. Spatial and interannual variability of dissolved organic matter in the Kolyma River, East Siberia, observed using satellite imagery. *J. Geophys. Res.* **2011**, *116*, 1–12. [[CrossRef](#)]
58. Osburn, C.L.; Stedmon, C.A. Linking the chemical and optical properties of dissolved organic matter in the Baltic–North Sea transition zone to differentiate three allochthonous inputs. *Mar. Chem.* **2011**, *126*, 281–294. [[CrossRef](#)]
59. McClelland, J.W.; Holmes, R.M.; Dunton, K.H.; Macdonald, R.W. The arctic ocean estuary. *Estuaries Coasts* **2012**, *35*, 353–368. [[CrossRef](#)]
60. Khosh, M.S.; McClelland, J.W.; Jacobson, A.D.; Douglas, T.A.; Barker, A.J.; Lehn, G.O. Seasonality of dissolved nitrogen from spring melt to fall freezeup in Alaskan Arctic tundra and mountain streams. *J. Geophys. Res. Biogeosci.* **2017**, *122*, 1718–1737. [[CrossRef](#)]
61. Mann, P.J.; Spencer, R.G.M.; Hernes, P.J.; Six, J.; Aiken, G.R.; Tank, S.E.; McClelland, J.W.; Butler, K.D.; Dyda, R.Y.; Holmes, R.M. Pan-arctic trends in terrestrial dissolved organic matter from optical measurements. *Front. Earth Sci.* **2016**, *4*, 25. [[CrossRef](#)]
62. Le Fouest, V.; Babin, M.; Tremblay, J.É. The fate of riverine nutrients on Arctic shelves. *Biogeosciences* **2013**, *10*, 3661–3677. [[CrossRef](#)]
63. Winterdahl, M.; Erlandsson, M.; Futter, M.N.; Weyhenmeyer, G.A.; Bishop, K. Intra-annual variability of organic carbon concentrations in running waters: Drivers along a climatic gradient. *Glob. Biogeochem. Cycles* **2014**, *28*, 451–464. [[CrossRef](#)]
64. Petrone, K.; Jones, J.; Hinzman, L.; Boone, R. Correction to “Seasonal export of carbon, nitrogen, and major solutes from Alaskan catchments with discontinuous permafrost”. *J. Geophys. Res.* **2006**, *111*, G02020. [[CrossRef](#)]
65. Stubbins, A.; Spencer, R.G.M.; Mann, P.J.; Holmes, R.M.; McClelland, J.W.; Niggemann, J.; Dittmar, T. Utilizing colored dissolved organic matter to derive dissolved black carbon export by arctic rivers. *Front. Earth Sci.* **2015**, *3*, 63. [[CrossRef](#)]
66. Jasechko, S.; Kirchner, J.W.; Welker, J.M.; McDonnell, J.J. Substantial proportion of global streamflow less than three months old. *Nat. Geosci.* **2016**, *9*, 126–129. [[CrossRef](#)]
67. McGuire, K.J.; McDonnell, J.J.; Weiler, M.; Kendall, C.; McGlynn, B.L.; Welker, J.M.; Seibert, J. The role of topography on catchment-scale water residence time. *Water Resour. Res.* **2005**, *41*. [[CrossRef](#)]
68. Kutscher, L.; Mörrh, C.-M.; Porcelli, D.; Hirst, C.; Maximov, T.C.; Petrov, R.E.; Andersson, P.S. Spatial variation in concentration and sources of organic carbon in the Lena River, Siberia. *J. Geophys. Res. Biogeosci.* **2017**, *122*, 1999–2016. [[CrossRef](#)]
69. Spencer, R.G.M.; Hernes, P.J.; Ruf, R.; Baker, A.; Dyda, R.Y.; Stubbins, A.; Six, J. Temporal controls on dissolved organic matter and lignin biogeochemistry in a pristine tropical river, Democratic Republic of Congo. *J. Geophys. Res.* **2010**, *115*, G03013. [[CrossRef](#)]
70. Lehn, G.O.; Jacobson, A.D.; Douglas, T.A.; McClelland, J.W.; Barker, A.J.; Khosh, M.S. Constraining seasonal active layer dynamics and chemical weathering reactions occurring in North Slope Alaskan watersheds with major ion and isotope ( $\delta^{34}\text{S}\text{SO}_4$ ,  $\delta^{13}\text{C}\text{DIC}$ ,  $^{87}\text{Sr}/^{86}\text{Sr}$ ,  $\delta^{44}/^{40}\text{Ca}$ , and  $\delta^{44}/^{42}\text{Ca}$ ) measurements. *Geochim. et Cosmochim. Acta* **2017**, *217*, 399–420. [[CrossRef](#)]
71. Ågren, A.; Buffam, I.; Berggren, M.; Bishop, K.; Jansson, M.; Laudon, H. Dissolved organic characteristics in boreal streams in a forest-wetland gradient during the transition between winter and summer. *J. Geophys. Res. Biogeosci.* **2008**, *113*, G03031. [[CrossRef](#)]
72. Creed, I.F.; Beall, F.D. Distributed topographic indicators for predicting nitrogen export from headwater catchments. *Water Resour. Res.* **2009**, *45*, W10407. [[CrossRef](#)]
73. Smith, L.; Beilman, D.; Kremenetski, K.V.; Sheng, Y.; MacDonald, G.; Lammers, R.; Shiklomanov, A.; Lapshina, E. Influence of permafrost on water storage in West Siberian peatlands revealed from a new database of soil properties. *Permafr. Periglac. Process.* **2012**, *23*, 69–79. [[CrossRef](#)]
74. Yi, Y.; Gibson, J.J.; Hélie, J.-F.; Dick, T.A. Synoptic and time-series stable isotope surveys of the Mackenzie River from Great Slave Lake to the Arctic Ocean, 2003 to 2006. *J. Hydrol.* **2010**, *383*, 223–232. [[CrossRef](#)]
75. Royer, T.V.; David, M.B. Export of dissolved organic carbon from agricultural streams in Illinois, USA. *Aquat. Sci.* **2005**, *67*, 465–471. [[CrossRef](#)]

76. Prokushkin, A.S.; Pokrovsky, O.S.; Korets, M.A.; Rubtsov, A.V.; Titov, S.V.; Tokareva, I.V.; Kolosov, R.A.; Amon, R.M.W. Sources of dissolved organic carbon in rivers of the Yenisei river basin. *Dokl. Earth Sci.* **2018**, *480*, 763–766. [[CrossRef](#)]
77. Meyer, J.; Tate, C. The effects of watershed disturbance on dissolved organic carbon dynamics of a stream. *Ecology* **1983**, *64*, 33–44. [[CrossRef](#)]
78. McClelland, J.W.; Townsend-Small, A.; Holmes, R.M.; Feifei Pan, M.S.; Khosh, M.; Peterson, B.J. River export of nutrients and organic matter from the North Slope of Alaska to the Beaufort Sea. *Water Resour. Res.* **2014**, *50*, 1823–1839. [[CrossRef](#)]
79. Pokrovsky, O.S.; Manasypov, R.M.; Loiko, S.; Shirokova, L.S.; Krickov, I.A.; Pokrovsky, B.G.; Kolesnichenko, L.G.; Kopysov, S.G.; Zemtsov, V.A.; Kulizhsky, S.P.; et al. Permafrost coverage, watershed area and season control of dissolved carbon and major elements in western Siberian rivers. *Biogeosciences* **2015**, *12*, 6301–6320. [[CrossRef](#)]



© 2019 by the authors. Licensee MDPI, Basel, Switzerland. This article is an open access article distributed under the terms and conditions of the Creative Commons Attribution (CC BY) license (<http://creativecommons.org/licenses/by/4.0/>).